Bismuth activation with quasi-Maxwellian neutrons at $kT \sim 30$ keV

A. Shor,[1] M. Tessler,[2] A. Plompen,[3] A. Arenshtam,[1] O. Aviv,[1] D. Berkovits,[1] M. Brandis,[1] Y. Eisen,[1] I. Eliyahu,[1] G. Feinberg,[1] M. Friedman,[2] S. Halfon,[1] M. Hult,[3] B. Kaizer,[1] D. Kijel,[1] A. Krása,[4] A. Kreisel,[1] T. Palchan,[2] M. Paul,[2] A. Perry,[1] I. Silverman,[1] S. Vaintraub,[1] and L. Weissman[1]

[1]*Soreq Nuclear Research Center, Yavne 81800, Israel*

[2]*Racah Institute of Physics, Hebrew University, Jerusalem 91904, Israel*

[3]*European Commission, Joint Research Centre, Retieseweg 111, 2440 Geel, Belgium*

[4]*Belgian Nuclear Research Centre SCK•CEN, Boeretang 200, 2400 Mol, Belgium*

(Received 20 July 2017; revised manuscript received 10 September 2017; published 15 November 2017)

Bismuth capture of neutrons is the termination point of the *s*-process cycle of nucleosynthesis in stellar environments. A new measurement is reported here for neutron activation of bismuth with an intense quasi-Maxwellian neutron source at $kT \sim 30$ keV. The measurement was performed at the SARAF phase I accelerator facility by bombarding a 1.5-mA proton beam on the liquid-lithium larget. The cross section of the ^{209}Bi(n,γ) capture reaction leading to the ^{210}Bi ground state was determined by combining β measurements from the ^{210g}Bi decay and α and γ from the subsequent ^{210}Po decay, along with detailed Monte Carlo simulations of the ^{7}Li(p,n) reaction kinematics and the activation experimental setup. Deduced Maxwellian averaged cross sections (MACS) for ^{209}Bi$(n,\gamma)^{210g}$Bi at $kT = 30$ keV using the ENDF, JEFF, and JENDL databases for the corrections and extrapolations yielded a value of 1.84 ± 0.09 mb. A comparison is made with previous measurements, including time-of-flight (TOF) measurements of the total bismuth capture cross section. Plans for obtaining the MACS for capture to the bismuth-210 metastable state in the reaction ^{209}Bi$(n,\gamma)^{210m}$Bi are discussed, along with estimates based on our results in comparison with TOF measurements. The bismuth neutron activation cross section is also of importance for design of GenIV reactor coolant and subcritical accelerator driven systems, especially in light of the 3 million year half-life of the ^{210m}Bi isomer.

DOI: 10.1103/PhysRevC.96.055805

I. INTRODUCTION

Bismuth is the last long-lived nuclide along the *s*-process reaction path for nucleosynthesis of the heavy elements in stellar environments [1]. Neutron capture on bismuth and beyond populates α-unstable isotopes contributing to the recycling of lighter nuclides involved in the *s* process [2]. While data on neutron capture exists, measurements on bismuth either lack sufficient accuracy or are not entirely consistent with each other. More precise measurements of neutron capture on bismuth are therefore needed for a more complete picture of the abundances near the end of the *s* process. Better knowledge of *s*-process abundances is also crucial for assessing radiogenic contributions due to Th/U decay and its use as cosmochronometers [3].

Neutron capture on bismuth is also of interest for planning and design of GenIV reactors. Eutectic Pb-Bi mixtures are planned as reactor coolants and as high power targets for intense proton/deuteron beams. The Pb-Bi mixture has the advantageous properties of low melting and high boiling point temperatures, in addition to chemical inertness, and low neutron moderation but large scattering cross sections. As such it is a very appropriate material for use as reactor coolants or for spallation targets for accelerator driven systems [4]. However, neutron capture on bismuth results in the radiotoxicity of the eutectic mixtures, with short-lived radiotoxicity due to the ^{210}Po and long-lived radiotoxicity due to the ^{210m}Bi isomer created. More precise data on neutron bismuth activation, especially leading to the long-lived isomer, is therefore crucial for reliable reactor design.

Figure 1 shows the scheme for neutron capture on bismuth and the possible decay schemes [5,6]. Neutron capture on ^{209}Bi ($I^\pi = 9/2^-$) can either result in creation of ^{210g}Bi in the ground state ($I^\pi = 1^-$), which decays to ^{210}Po with a half-life of 5.012 days, with the ^{210}Po subsequently α decaying to ^{206}Pb with a 138-day half-life. A small fraction [branching ratio of $1.23(4) \times 10^{-5}$ [6]] of the ^{210}Po decays to the ^{206}Pb* excited state, with the subsequent emission of a γ ray with energy of 803 keV. The second branch is the creation of a long-lived isomer ^{210m}Bi ($I^\pi = 9^-$), a metastable state at excitation energy of 271 keV, with the ^{210m}Bi α decaying to ^{206}Tl with a 3 million year half-life.

Several measurements of neutron activation of bismuth have been performed with cold and thermal neutrons [7,8], neutrons in the resonance region [9–12], neutrons with quasi-Maxwellian distribution at $kT \sim 30$ keV [13,14], and neutrons at $\sim$500 keV [15]. These measurements have also been compared to evaluated activation cross sections [16–18]. A disparity exists between the different measurements and also between the evaluated cross sections. There is therefore a need for improvement on the accuracy and/or consistency between these measurements, especially regarding comparisons between activation to the bismuth ground state and the metastable state.

We report on a new measurement of activation of bismuth with intense quasi-Maxwellian neutrons at the Soreq Applied Research Accelerator Facility (SARAF) and the Liquid Lithium Target (LiLiT). β measurements from irradiated bismuth samples have been performed for the ^{210g}Bi decay, and α and γ measurements for the subsequent ^{210}Po decay. The

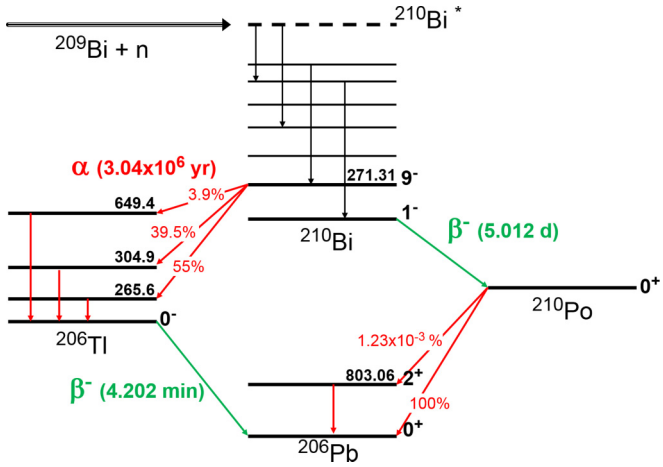

FIG. 1. Decay scheme following neutron capture on ^{209}Bi. Energy level data from [5,6].

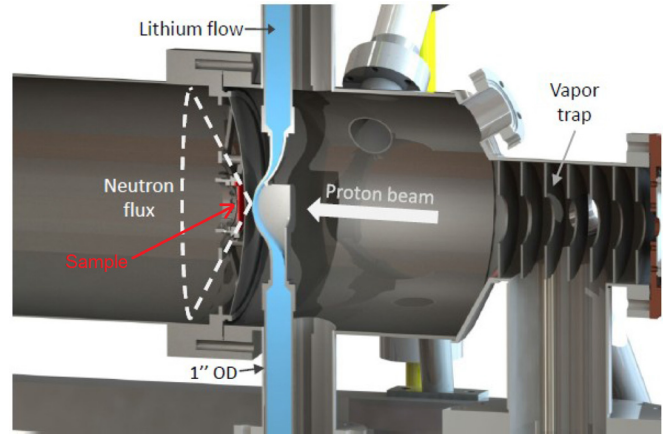

FIG. 2. Schematic diagram of the liquid-lithium target (LiLiT) and activation target assembly, as described in text.

results obtained for all three activities are consistent with each other, and combining the three results provides a cross section measurement with uncertainty of ∼5%. Detailed Monte Carlo simulations of the ^{7}Li(p,n) reaction kinematics and the beam + target + sample geometry are made to determine systematic corrections necessary for derivation of Maxwellian averaged cross sections (MACSs) and comparison with several different cross section libraries. We also discuss existing limitations for extracting data on activation of the ^{210m}Bi and future plans for possible accelerator mass spectrometry (AMS) measurements with existing irradiated bismuth samples.

The outline of this paper is as follows. Section II describes the experimental setup, including the SARAF-LiLiT facility and the α-β and γ detection systems used. Section III discusses the activation measurements of the irradiated bismuth samples. Section IV discusses the data analysis and cross section derivations, including the Monte Carlo simulations and extracted neutron spectrum, and the extrapolations of the MACSs. Section V contains discussion of the results and comparison with existing data and prospects for future measurements. Section VI contains a summary of the measurement reported here.

II. EXPERIMENTAL PROCEDURE

A. Bismuth activation at SARAF-LiLiT

The experimental work was performed at the recently commissioned Soreq Applied Research Accelerator Facility (SARAF) radio-frequency (RF) linear accelerator [19] and the high power Liquid-Lithium Target (LiLiT) [20]. SARAF Phase I consists of an electron cyclotron resonance (ECR) ion source and low energy beam transport (LEBT), a four-rod-type radio-frequency quadrupole (RFQ), a prototype superconducting cryomodule (PSM) consisting of three solenoids and six half-wave resonators operating at 176 MHz, a diagnostic plate (D plate), and a magnetic beam line to guide the beam to the internal liquid lithium target. The LiLiT target provides liquid lithium circulation via an electromagnetic pump circulating the liquid lithium to an appropriately designed nozzle which provides a 1.5-mm-thick flow of liquid lithium just upstream of the samples to be irradiated. The lithium flow is in the accelerator vacuum while the secondary bismuth target is a few millimeters downstream of the lithium jet in a separated vacuum chamber. At proton energy of 1928 keV, about 3.9×10^{10} quasi-Maxwellian neutrons are produced per second per mA; approximately 88% of the neutrons (3.4×10^{10}) are incident on the irradiated samples used in this measurement. Present capabilities of the phase I machine allows for continuous wave (CW) acceleration of protons at 1.5–2 mA and at energies of up to 4 MeV, and pulsed deuterons up to 5 MeV. Phase II, planned for 2023 [21], will include four additional cryomodules containing half-wave resonators and will enable CW acceleration of protons or deuterons at currents of up to 5 mA and at energies of up to 40 MeV.

The bismuth activation with quasi-Maxwellian neutrons relies on a technique developed at Forschungszentrum Karlsruhe for obtaining stellarlike distributions by taking advantage of kinematics for near threshold two-body reactions producing neutrons. In particular, the ^{7}Li(p,n) reaction near threshold on a thick lithium target produces neutrons kinematically boosted in the laboratory frame with an energy distribution similar to that associated with asymptotic giant brach (AGB) stars at kT of ∼30 keV, and kinematically focused in a forward-going cone of about ±60°. This technique has been extensively used, in conjunction with time-of-flight (TOF) technique, to determine reaction rates in stellar environments relevant to the s process of nucleosynthesis [22].

The advantage of the SARAF-LiLiT facility is the availability of intense quasi-Maxwellian neutrons of more than an order of magnitude higher than previously attainable. This requires special target arrangements and beam tune procedures. Details on the beam tune procedures and the special target configuration can be found in Refs. [23] and [24]. We briefly summarize this procedure as applied to the measurements described in this paper. Figure 2 shows a schematic diagram of the experimental setup. The 7-mm-diameter proton beam impinges on the free-surface lithium film. The bismuth sample(s), along with gold foil(s) used for normalization, were mounted on a holder and positioned

in the outgoing neutron cone at a distance of 7 mm from the lithium surface in a vacuum chamber separated from the LiLiT chamber by a 0.5-mm stainless steel wall convex to the beam. The LiLiT vacuum vessel contained several ports with line of sight to the proton-lithium interaction area. A lithium vapor trap minimizes the lithium vapor level in the accelerator vacuum.

A ∼1.5-mA proton beam was accelerated and focused onto the lithium target. The energy of the proton beam was measured by Rutherford backscattering apparatus and by time of flight between beam pickup monitors (BPMs), both sets of detectors situated in the D plate downstream of the PSM. The beam energy for this measurement was determined to be 1928 ± 3 keV, where the uncertainty is due to the uncertainty in the RBS fit and the distance between the two sets of BPM detectors. While the mean proton energy was measured with satisfactory precision, the proton beam energy profile had a moderate energy spread, as is characteristic of an RF linac. The energy spread was measured several ways. A threshold curve was performed for the Li(p,n) reaction, for which the energy threshold is at $E_p = 1880.4$ keV. The energy spread was also measured via an energy scan on a ^{13}C target around the ^{13}C(p,γ) resonance at 1747 keV. The proton energy profile was also determined by measuring the longitudinal beam projection as a function of the phase of the downstream half-wave resonator, and using beam dynamics formalism to extract the energy profile. All three techniques gave a proton energy spread of about 15 keV rms. Further details of these studies can be found in Ref. [25].

For studying bismuth activation, several experimental runs were performed, mostly with stacks of 2-mm-thick bismuth plates in an effort to understand the systematics for optimizing measurements on activation of the ^{210m}Bi metastable state isomer. It was realized, however, that while neutron capture on bismuth is very small, the elastic scatter cross section is rather large, and activation with a thick bismuth stack involves considerable multiple scattering which complicates the activation profile, and lowers the effective energy distribution of the captured neutrons. It was therefore decided that for accurate measurement of neutron capture cross section to the ^{210g}Bi ground state, a minimal thickness for the activation sample is desired.

Two bismuth activation runs were performed dedicated to measuring neutron capture leading to ^{210g}Bi in the ground state. The first involved a 1-μm-thick bismuth layer with nominally 99.97% pure bismuth sputtered onto a 0.25-mm mylar foil [26]. This activation was performed for measuring the β's from the ^{210g}Bi and the α's from the subsequent ^{210}Po decay. The bismuth thickness was measured using Rutherford backscattering techniques at the Bar-Ilan University RBS facility [27], and was found to be of thickness $(2.86 \pm 0.12) \times 10^{18}$ atoms/cm^2. A 12.1-μm-thick gold foil was placed 0.7 mm upstream of the bismuth foil. The gold activation was used for monitoring the neutron fluence based on the well-known ^{197}Au(n,γ) cross section [28,29]. Both foils were of area 25 mm×25 mm. Due to slight beam steering, the 7-mm-diameter beam was offset about 3 mm from the center as measured by autoradiography of the gold foils. See Ref. [30] for details about the autoradiography procedures. During the course of the experimental run a total proton charge of 4.2 mA h was accumulated incident on the liquid lithium target.

The second bismuth activation was for measuring capture to the ^{210g}Bi ground state using the decay branch leading to the 803-keV γ from the ^{210}Po decay (see Fig. 1). Since the branching ratio for the $^{210}\text{Po} \rightarrow {}^{206}\text{Pb}^* \rightarrow {}^{206}\text{Pb} + \gamma$ is on the order of $\sim 10^{-5}$, we required a rather thick 2-mm bismuth sample for sufficient amount of activated nuclei. The thickness of the bismuth target in atoms/cm^2 was determined by weighing the sample and dividing by the area. The bismuth sample was purchased from Princeton Scientific, and was specified with purity of 99.9999% [31]. Corrections for scattering in the thick bismuth target were estimated with the help of the simulations codes discussed below. The activation was done with two gold foils for normalization, one directly upstream and one downstream of the bismuth slab. This second run involved an accumulation of 4.0 mA h of proton charges on the liquid lithium target.

B. Setup for α and β measurements

The α and β measurements from the activated 1-μm bismuth foil were performed with a Canberra shielded iSolo500L detection system containing a 2000-mm^2 500-μm-thick PIPS silicon detector [32]. The bismuth foil was of area 25×25 mm^2, well within the 50-mm-diameter area of the PIPS detector. The sample was placed on a tray, and when closed, was on axis and at a distance of 7.8 mm beneath the detector. The measuring compartment was not in vacuum, therefore multiple scattering and energy loss affected the distribution of α's and β's. This broadening of the α peaks was well matched with the morphology of the samples, where the sputtered bismuth atoms' penetration of up to several microns into the mylar substrate also resulted in comparable multiple scattering of the α's and β's.

The α efficiency of the iSolo detection system was calibrated with an Eckert and Ziegler triple α source [33] with α peaks at 5.1, 5.5, and 5.8 MeV (from ^{239}Pu, ^{241}Am, and ^{244}Cm sources); these energies are close to the ^{210}Po α decay energy of 5.3 MeV. The source was 7 mm in diameter, with the activity calibrated to within an accuracy of ±1.5%. An x-y scan of the detection area with the calibrated source was made to determine the variation of the detector efficiency over the area of the activated bismuth sample, although the variations were small due to the large area of the PIPS detector. A pulse height threshold of 2 MeV equivalent (taking into account energy loss in the air) was made to reject the β contribution when measuring the activated bismuth sample. The α efficiency averaged over the relevant area was found to be (35.5 ± 0.7)%, where the error includes averaging over activated region.

The efficiency for β's from the activated bismuth sample was calibrated in a self-consistent manner. The gold foil activated simultaneously with the bismuth foil was measured for activity from the ^{198}Au isotope with a calibrated high purity germanium (HPGe) detector with an accuracy of ±1.5%. We waited for several weeks to allow the gold foil activity to be reduced, so that we could measure the same gold foil with the iSolo500L detector for β's from the ^{198}Au decay.

The efficiency for β's of the irradiated gold foil, based on the comparison with the γ measurements made with the same activated foil, was determined to be $(29.2 \pm 0.7)\%$. Corrections for the β efficiency for the activated bismuth foil, as compared to the measured activated gold foil, was determined with a detailed simulation using the Geant4 [38] simulation package, where the simulation included β spectrum from the respective targets, foil geometry, energy loss, multiple and back scattering in the foil and air, and detector energy threshold. The result of these corrections gave us a β efficiency for the activated bismuth foil of $(27.4 \pm 1.0)\%$.

C. Setup for γ measurements

The γ measurements for the activated 2-mm bismuth slab were made with a well shielded 70% p-type coaxial Canberra HPGe detector. The shield consisted of periphery of lead shielded with an inner tin liner, both with a low level of radioactive impurities, surrounded with scintillators that provide anticoincidence signals for cosmic rays. The γ background level inside the shielded detector is about three orders of magnitude smaller than typical unshielded surface γ background. This low background was necessary for clear identification of the 803-keV peak given the 1.23×10^{-5} branching ratio for this decay scheme. Detector efficiency at contact was determined with a calibrated γ source, with interpolation techniques between measured lines, and consistency check with a dedicated detector simulation code. Monte Carlo simulations were performed for accurate assessment of finite sample size and bismuth self-absorption of the 803-keV γ's. Details on this low background HPGe detector system and simulations can be found in Ref. [34].

III. BISMUTH IRRADIATION AND ACTIVATION MEASUREMENTS

The two sets of bismuth irradiations at SARAF-LiLiT summarized in this paper involved irradiation over the course of about 3.5 h each and accumulation of about 4.2 and 4.0 mA h of protons on the liquid lithium target for the bismuth foil and thick bismuth target, respectively. At incident proton energy E_p of 1928 keV, a total accumulated neutron fluence of about 5.1×10^{14} and 4.9×10^{14} neutrons on target for each experimental run was obtained.

Immediately following the first irradiation involving the thin bismuth foil, the activated bismuth foil was removed from the target assembly, transported to the detection laboratory, and placed in front of a calibrated HPGe detector to detect possible activation of impurities which may contaminate the β^- spectrum to be measured. In addition to several short lived species, significant signals from the 564.2- and 692.6-keV lines from ^{122}Sb decay ($\tau_{1/2} = 2.7$ d) were observed, produced by neutron capture on a stable nuclide of ^{121}Sb, apparently an impurity contained in the bismuth foil (or mylar). It is assumed that since impurities of antimony were present, then we should also expect comparable activation of ^{124}Sb ($\tau_{1/2} = 60.2$ d), produced by neutron capture on stable nuclide ^{123}Sb, although γ lines associated with ^{124}Sb were not seen, presumably because of the relatively long half-life. Both antimony isotopes are β emitters so contamination to the β spectrum should be anticipated. In addition, the 847- and 1811-keV lines from ^{56}Mn were observed, apparently from manganese impurities in the aluminum frame used for holding the bismuth foil. Following measurements for γ emitters, the bismuth foil was placed in the iSolo α/β detection compartment and acquisition started for a 30-day-long α and β activity measurement. The gold foil that had been activated along with the bismuth foil was then measured with the calibrated HPGe detector to determine the ^{198}Au activity via the 411.8-keV line that serves as normalization for the bismuth activation measurement.

The second irradiation at SARAF commenced with the thick bismuth target sandwiched between two gold foils. The objective for the thick bismuth sample was to measure the 803-keV γ line (branching ratio of 1.23×10^{-5}) from the ^{210}Po decay ($\tau_{1/2} = 138$ d) following the ^{210}Bi decay ($\tau_{1/2} = 5.012$ d). We waited 25 days (five ^{210}Bi half-lives) before placing the activated thick bismuth target in the low background HPGe detector system. Prominent in the γ spectrum was the 569.7- and the 1063.7-keV γ lines from ^{207}Bi ($\tau_{1/2} = 32.9$ yr). We concluded that the ^{207}Bi is formed due to ^{209}Bi$(\gamma,2n)$ reactions with the 14.6- and 17.6-MeV high energy γ rays produced in the $p + $Li reaction with the thick liquid lithium target [24]. This effect essentially dismisses our original intention of long irradiations with thick stack of bismuth slabs in the hope of observing the 266- and 305-keV γ lines from decay of ^{210m}Bi, and thereby measure activation to the ^{210ms}Bi metastable state with Maxwellian neutrons in the SARAF-LiLiT facility. The two gold foils sandwiching the bismuth slab were measured following the irradiation with a calibrated HPGe detector and used for normalization of the bismuth activation.

A. Gold foil activity

The technique of simultaneous activation of gold foils along with the samples of interest has been developed as a source of normalization with a known reference standard. The gold reference standard has been utilized for normalization of activation with quasi-Maxwellian neutrons, since precise measurements exist for both cross sections as a function of energy for the ^{197}Au$(n,\gamma)^{198}$Au reaction and averaged cross section obtained with a Maxwell-Boltzman distributions, as discussed in the literature [29,35].

Following irradiation, the gold foils were measured with a calibrated HPGe detector at a distance of 20 cm to keep finite size effects negligible, and a Gaussian fit was made for the 411.8-keV line. The number of ^{198}Au nuclei activated during the irradiation was determined according to the following equation:

$$N_{Au198} = \frac{S_\gamma(E)}{I_\gamma(E)\varepsilon_\gamma(E)} \frac{t_{\text{real}}}{t_{\text{live}}} \frac{\exp(\lambda t_{\text{cool}})}{1-\exp(\lambda t_{\text{real}})} \frac{\lambda t_{irr}}{1-\exp(\lambda t_{irr})}, \quad (1)$$

where $S_\gamma(E)$ is the area of the fitted peak area, $I_\gamma(E)$ is the emission probability ($\sim$0.96), $\varepsilon_\gamma(E)$ is the detector efficiency, and $\lambda = 1/\tau$ is the decay constant. The times involved are the sample irradiation time t_{irr}, the cooling time following

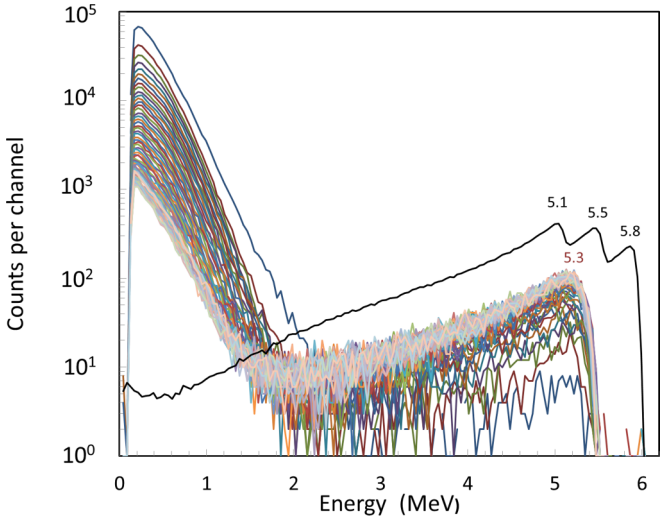

FIG. 3. Spectra of irradiated bismuth foil with iSolo counter showing β and α contributions. Consecutive data acquisitions of 12-h duration each were collected over a span of 30 days. Superimposed is the spectrum obtained with the triple-α calibration source.

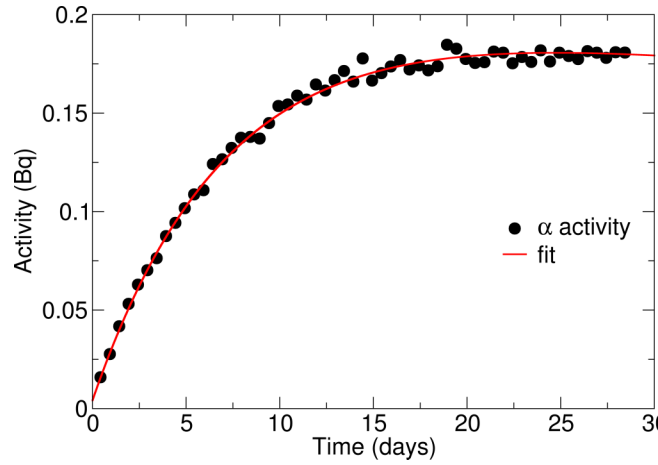

FIG. 4. α activity time evolution for the irradiated bismuth foil.

irradiation prior to measurement t_{cool}, and the measurement real and live time t_{real} and t_{live}.

The bismuth foil was irradiated along with a 12.1 ± 0.1-μm-thick gold foil. The total number of activated ^{198}Au nuclei immediately following irradiation was $(3.06 \pm 0.05) \times 10^{10}$. The irradiation of the 2-mm-thick bismuth target consisted of two gold foils, one directly before ($12.1 \pm 0.1\ \mu$m thick) and the second directly after ($13.4 \pm 0.1\ \mu$m thick) the bismuth target. The total number of activated ^{198}Au nuclei immediately following irradiation for these gold foils was $(2.93 \pm 0.05) \times 10^{10}$ and $(2.49 \pm 0.05) \times 10^{10}$ for the upstream and downstream gold foils, respectively. The difference of the activity level was borne out by SimLiT-GEANT4 simulations (ratio of $\sim$0.77, normalized to foil thickness), and is due to the slightly increased distance from the production target and also to elastic scattering of the neutrons in the thick bismuth. For normalization of the 2-mm-thick bismuth target, the weighted average of the activity of two gold foils was used.

B. Bismuth foil activity

Measurements of the activated bismuth foil were made with the iSolo500L shielded β-α counter. We performed 60 consecutive half-day accumulations over the course of 30 days. Figure 3 shows the energy spectra obtained by the iSolo counter for the 60 runs taken during the 30-day measurement period. Note that the low energy β contribution is at maximum for the early runs and becomes progressively smaller, whereas the α contribution begins at zero and grows progressively for subsequent runs. Superimposed is the spectrum we obtained with the triple α source, which determined the energy calibration. The broadening of the α energy peaks is the result of 8 mm of air, and the depth of the bismuth embedded in the mylar substrate. The large solid angle of the detector with respect to the source also contributed to the energy broadening. Nonetheless, the α-β distinction is very clear. The cut at 2-MeV equivalent pulse height to separate between β's and α's proved very effective, as minor shifts of the cut location results in negligible differences in efficiencies.

C. α activity

The evolution of the α activity with time following irradiation of the bismuth foil as measured by the iSolo detector is shown in Fig. 4. The data points represent the average α activity per 12-h measuring period obtained by taking the total counts in the α region of the spectra, divided by the accumulation time, and correcting for the α efficiency. The time t is taken from the end of irradiation up to the middle of the activity measurement. The α activity plot was fit with the following formula:

$$A_\alpha(t) = N_{Bi210}(t_{irr}) \frac{\lambda_\beta \lambda_\alpha}{\lambda_\beta - \lambda_\alpha} [f_{irr} \exp(-\lambda_\alpha t) - \exp(-\lambda_\beta t)], \tag{2}$$

where $\lambda_\beta = 1/\tau_\beta$ is the decay constant of $^{210gs}\text{Bi} \rightarrow {}^{210}\text{Po} + \beta^-$, and $\lambda_\alpha = 1/\tau_\alpha$ is the decay constant of $^{210}\text{Po} \rightarrow {}^{206}\text{Pb} + \alpha$. The correction factor f_{irr} is the correction for ^{210}Bi decay during irradiation, given by $f_{irr} = 1 + (\lambda_\beta - \lambda_\alpha) t_{irr}/2$. Corrections for decay during the measuring time are insignificant for t taken to the middle of the activity measurement. The goodness of fit of the α activity with Eq. (2) yields an adjusted R square of 0.995, indicating there was no α emitter other than the ^{210}Po.

The maximal α activity derived from the measurements is given by

$$A_\alpha = N_{Bi210}(t_{irr}) \frac{\lambda_\beta \lambda_\alpha}{\lambda_\beta - \lambda_\alpha} = 0.2135 \pm 0.0034\ Bq,$$

where the error consists of $\pm 1.5\%$ α calibration error and $\pm 0.5\%$ error due to the fit.

The total number of ^{210g}Bi nuclei at the end of irradiation, as derived from the α activity, is

$$N^{\alpha}_{Bi210}(t_{irr}) = (3.46 \pm 0.05) \times 10^6 \text{ atoms}.$$

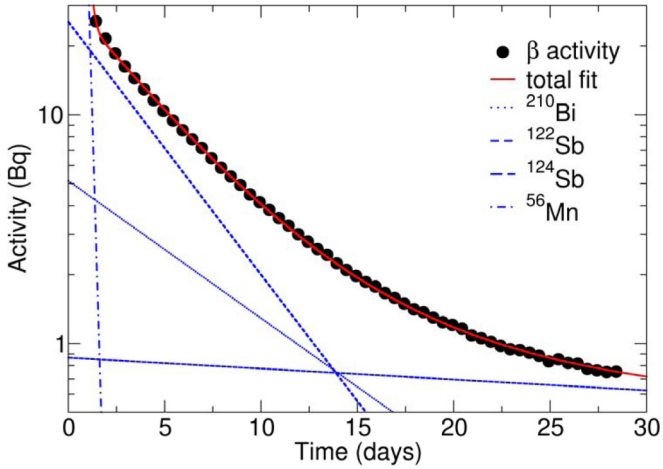

FIG. 5. β activity time evolution for the irradiated bismuth foil, showing contributions from ^{210}Bi, ^{56}Mn, ^{122}Sb, and ^{124}Sb decay.

D. β activity

The evolution of the β activity with time following irradiation of the bismuth foil as derived from the iSolo measurements is shown in Fig. 5, where the β's were defined as events below effective energy of 2 MeV and where the activity is corrected for β efficiency. The time development of the β activity does not show a pure exponential decay, an indication of activation of impurities that contribute to the β activity. As discussed above, γ lines from the ^{122}Sb and from the ^{56}Mn isotopes were observed with the HPGe detector right after activation, indicating significant Sb impurities in the bismuth foil and aluminum frame, respectively. Other impurities with shorter half-lives were also observed, but they do not affect the β activity fit shown in Fig. 5. The β activity plot was fit with the following formula:

$$A_\beta(t) = A^\beta_{Bi210}(t_{irr})\exp(-\lambda_{Bi210}t) + A_{Mn56}(t_{irr}) \times \exp(-\lambda_{Mn56}t) + A_{Sb122}(t_{irr})\exp(-\lambda_{Sb122}t) + A_{Sb124}(t_{irr})\exp(-\lambda_{Sb124}t), \quad (3)$$

where $\lambda_{\mathrm{Bi210}} = 1/\tau_{\mathrm{Bi210}}$ is the decay constant for ^{210g}Bi $\rightarrow$ ^{210}Po $+ \beta^-$, $\lambda_{\mathrm{Mn56}} = 1/\tau_{\mathrm{Mn56}}$ is the decay constant for ^{56}Mn with half-life of 2.6 h, $\lambda_{\mathrm{Sb122}} = 1/\tau_{\mathrm{Sb122}}$ is the decay constant for ^{122}Sb with half-life of 2.7 days, and $\lambda_{\mathrm{Sb124}} = 1/\tau_{\mathrm{Sb124}}$ is the β decay constant for ^{124}Sb with half-life of 60.2 days.

The best minimum χ^2 fit to the β activity gives a contribution from the ^{210}Bi β decay of

$$A^\beta_{Bi210}(t_{irr}) = 5.14 \pm 0.49\ Bq,$$

where the error includes primarily a 9.3% error due to the fit and a 2.5% error for the β efficiency calibration.

The total activation to ^{210g}Bi at the end of irradiation, as derived from the β activity, is

$$N^\beta_{Bi210}(t_{irr}) = A^\beta_{Bi210}(t_{irr})\frac{1}{\lambda_{Bi210}} = (3.2 \pm 0.3) \times 10^6 \text{ atoms}.$$

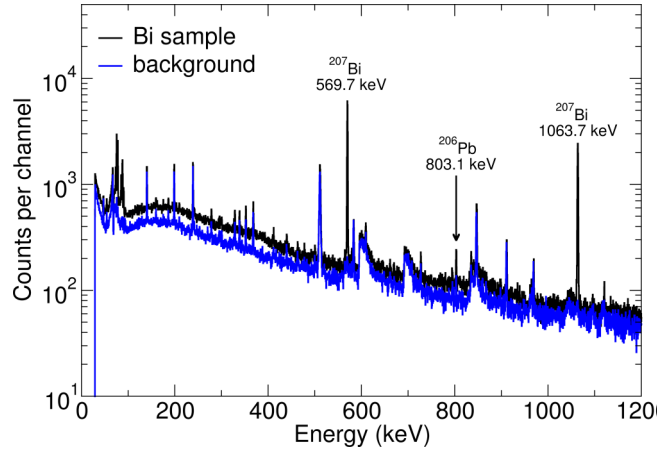

FIG. 6. γ spectrum from irradiated 2-mm-thick bismuth target in a low background shielded HPGe detector showing 803-keV line from the ^{210}Po $\rightarrow$ ^{206}Pb* $\rightarrow$ ^{206}Pb $+ \gamma_{803}$ decay and 569.7- and 1063.7-keV lines from ^{207}Bi decay. Background spectrum is also shown.

E. γ activity from thick Bi sample:

Measurement of the 803-keV γ line from the ^{210}Po $\rightarrow$ ^{206}Pb* $\rightarrow$ ^{206}Pb $+ \gamma_{803}$ reaction provides a consistency check on the α and β measurements. The low branching ratio of $\sim 10^{-5}$ for this decay branch, in addition to requiring a 2-mm-thick bismuth target for increased activated nuclei, also required a long γ measurement of the irradiated sample with shielded low background HPGe detector. We waited about 5 weeks for the ^{210g}Bi to decay to ^{210}Po, after which we commenced with the long γ measurement of the irradiated bismuth target over a period of about 12 days. A separate measurement of the HPGe background also over 12 days was performed for background subtraction. Despite the shielded low background environment, a faint signal from the 803-keV line from the background contribution of polonium was present. Figure 6 shows the γ spectrum obtained from the irradiated thick bismuth target, with a comparison of the low level background spectrum collected over comparable acquisition time. Prominent in the spectrum from the bismuth sample are the 569.7- and 1063.7-keV lines from ^{207}Bi produced in the ^{209}Bi$(\gamma,2n)$ reaction with the high energy γ'sproduced in the $p +$ Li reaction.

Figure 7 shows a section of the γ spectrum in the region of the 803-keV peak from the ^{210}Po $\rightarrow$ ^{206}Pb* $\rightarrow$ ^{206}Pb $+$ γ_{803} decay, and a Gaussian fit for the 803-keV peak. Also superimposed is the low level background taken over the same accumulation time, also showing traces of the 803-keV line and the fitted peak, where the background peak is presumably from impurities in the lead or copper radiation shield.

For the thick bismuth sample, the number of activated ^{210gs}Bi atoms at the end of irradiation is determined from the counts in the 803 γ peak, as given by the following formula:

$$S^{\mathrm{meas}}_\gamma(t) = N^\gamma_{Bi210}(t_{irr}) \times \frac{\lambda_\alpha\lambda_\beta}{\lambda_\beta - \lambda_\alpha} \times \varepsilon_\gamma \times \gamma_{b.r.} \times \gamma_{bi\text{-}abs} \times \gamma_{el\text{-}conv} \times [f_{irr}\exp(-\lambda_\alpha t) - \exp(-\lambda_\beta t)], \quad (4)$$

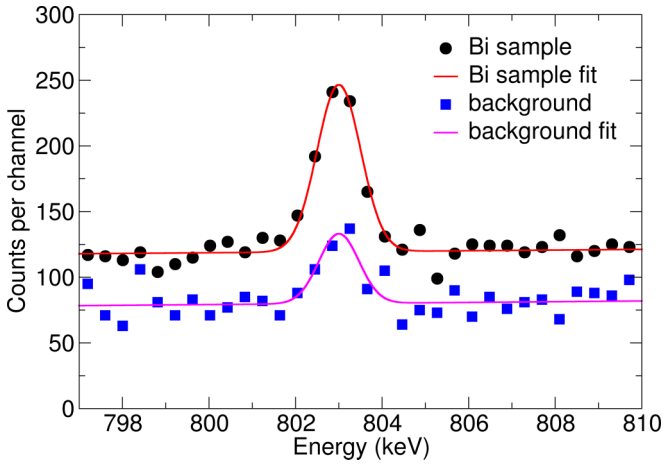

FIG. 7. γ spectrum and fit of the 803-keV peak from irradiated 2-mm-thick bismuth target. Background spectrum is also shown. Accumulation time for both spectra ∼12 days.

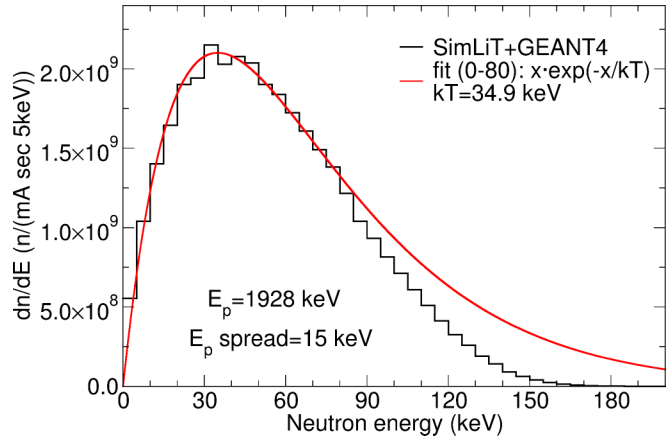

FIG. 8. Actual distribution of neutron flux $dn/dE_{\rm n}$ impinging the bismuth target, as simulated by SimLiT and Geant4. A best fit for Maxwellian in the region of 0–80 keV gives $kT = 34.9$ keV.

where $\lambda_\beta = 1/\tau_\beta$ is the decay constant of $^{210g}\mathrm{Bi} \rightarrow {}^{210}\mathrm{Po} + \beta^-$, and $\lambda_\alpha = 1/\tau_\alpha$ is the decay constant of $^{210}\mathrm{Po} \rightarrow {}^{206}\mathrm{Pb} + \alpha$. $\varepsilon_\gamma = 0.0696 \pm 0.002$ is the γ efficiency of the HPGe detector on contact for the 803-keV line, $\gamma_{\rm b.r.} = (1.23 \pm 0.04) \times 10^{-5}$ is the branching ratio for 803-keV γ line, $\gamma_{\rm el\text{-}conv} = 0.990 \pm 0.002$ is the correction for electron conversion. $\gamma_{\rm bi\text{-}abs} = 0.82$ is the self-absorption and geometry corrections for the 2-mm bismuth sample placed in direct contact with the HPGe detector, as determined by detailed Geant4 simulations. $S_\gamma^{\rm measured}$ is the total measured counts divided by the measurement time obtained from the fit of the 803-keV peak with the bismuth sample, minus the background count rate of the 803-keV peak obtained without the bismuth sample. The time t is taken from the end of the irradiation to the middle of the counting period.

The total activation to ^{210g}Bi for the 2-mm-thick bismuth sample at the end of irradiation, as derived from the measured counts for the 803 keV, is

$$N^{\gamma}_{Bi210}(t_{irr}) = (5.7 \pm 0.9) \times 10^9 \text{ atoms}$$

with the error primarily statistical, including subtraction of the background 803-keV peak signal.

IV. ANALYSIS AND RESULTS

A. Monte Carlo simulations and effective neutron spectrum

The $p + \mathrm{Li}$ reaction slightly above threshold has been used for producing a quasi-Maxwellian distribution at $kT \sim 30$ keV of neutrons kinematically focused to a $\pm 60^\circ$ cone. The reaction has been used extensively to simulate conditions in massive AGB stars for measuring reactions relevant to the s process of nucleosynthesis. However, deviations of the actual neutron spectra from a Maxwellian distribution and the actual experimental and sample geometry require resorting to detailed Monte Carlo simulations to understand the correction factors needed for accurately determining the MACS.

Accurate evaluation of the experimental cross sections and estimate of their systematic corrections, and especially extrapolations to the Maxwellian averaged cross sections, require a proper knowledge of the relevant neutron distribution and the convolution with elemental reaction cross sections. To properly correct for experimental systematics and enable extrapolation to different values of kT, we make extensive use of the simulation code SimLiT [36] to simulate the kinematics of neutrons produced in the $p + \mathrm{Li}$ thick target reaction. This code has been shown to reliably reproduce experimentally measured neutron spectra produced in the $p + \mathrm{Li}$ thick target reactions at various proton energies and neutron production angles [37]. In conjunction with GEANT4 [38], the computer programs provide for simulations of neutron production, transport, and scattering of the irradiated samples and holders. Further details on SimLiT and detailed Monte Carlo simulation with GEANT4 are to be found in Ref. [36].

We performed SimLiT-GEANT4 simulations for 10^7 neutrons incident on the bismuth sample. The input to the SimLiT program included the bombarding energy of the proton beam at $E_{\rm p} = 1928$ keV and energy spread of 15 keV rms, and Gaussian transverse profile of 2.7 mm rms. The input to GEANT4 was the detailed geometry of the experimental setup, including all support structures, scattering material, and bismuth sample geometry and location. The simulations calculate the actual distribution of neutron flux impinging the gold and bismuth samples, $\Phi_{\rm sim} = \frac{dn_{\rm sim}}{dE_n}$, shown in Fig. 8. Superimposed on the simulated distribution is a fit of a Maxwellian flux $dn/dE_{\rm n} \sim E_{\rm n} \times \exp(-E_{\rm n}/kT)$, with the fit performed for the region of 0–80 keV, and providing a best fit for $kT = 34.9$ keV.

B. Determination of the experimental cross section

The experimental cross section for activation of the bismuth sample, for the given distribution of neutrons impinging on the bismuth sample, is obtained by comparing the bismuth and gold activation, normalized by the number of atoms in the respective samples, and multiplied by the average gold cross section obtained by convoluting the calculated neutron distribution impinging the gold target with known cross sections for the $^{197}\mathrm{Au}(n,\gamma)^{198}\mathrm{Au}$ reaction. For example, the

experimental cross section for ^{209}Bi$(n,\gamma)^{210g}$Bi as measured by the α's from the ^{210}Po decay, averaged over the neutron energy distribution given in Fig. 8, is given by

$$\sigma^{\alpha}_{\rm exp}(^{210g}{\rm Bi}) = \sigma_{\rm exp}({\rm Au})\frac{N^{\alpha}_{Bi210}}{N_{Au198}}\frac{N_{Au197}}{N_{Bi209}}\frac{\bar{\Phi}_{Au198}}{\bar{\Phi}_{Bi210}}, \quad (5)$$

where N_{197Au} and N_{209Bi} are the target thicknesses in atoms/cm^2 for the gold and bismuth foils, respectively, N^{α}_{Bi210} and N_{Au198} are the number of activated nuclei following irradiation in each foil, and $\bar{\Phi}_{Bi210}$ and $\bar{\Phi}_{Au198}$ are the neutron fluences averaged over the volume of the samples as determined by SimLiT-Geant4 for each of the foils. The effective experimental cross section for ^{198}Au averaged over the neutron energy distribution in the gold target is derived using

$$\sigma_{\rm exp}({\rm Au}) = \int \sigma_{\rm ENDF}(E_n,{\rm Au})\frac{dn_{\rm sim}}{dE_n}dE_n \Big/ \int \frac{dn_{\rm sim}}{dE_n}dE_n, \quad (6)$$

where the cross sections for ^{197}Au$(n,\gamma)^{198}$Au as a function of neutron energy is taken from the newly revised ENDF/B-VIII.b4 [16]. Convolutions with this newly revised library gives averaged cross sections for the gold approximately 1% large than with the somewhat older ENDF/B-VII.1 or JENDL-4.0 [17] evaluation libraries. For the neutron spectrum shown in Fig. 8, the experimental gold cross section obtained from convoluting with the ENDF evaluated cross section is $\sigma_{\rm exp}({\rm Au}) = 583$ mb. This is to be compared to a spectrum averaged cross section of 502 mb for a purely Maxwellian neutrons distribution at $kT = 35$ keV, where the larger average cross section for the simulated neutron spectrum shown in Fig. 8 is due to the fewer events in the high energy tail and thereby more emphasis on the resonance region at lower energies which exhibit higher cross sections.

Using the above formalism, we obtain the following experimental cross section for the bismuth activation to the ^{210gs}Bi ground state, averaged over the neutron spectrum impinging the bismuth target, as measured by α, β, and γ decay, normalized with the gold experimental cross section as above:

$$\sigma^{\alpha}_{\rm exp}(^{210g}{\rm Bi}) = 1.67 \pm 0.07 \text{ mb},$$
$$\sigma^{\beta}_{\rm exp}(^{210g}{\rm Bi}) = 1.55 \pm 0.14 \text{ mb},$$
$$\sigma^{\gamma}_{\rm exp}(^{210g}{\rm Bi}) = 1.8 \pm 0.3 \text{ mb}.$$

These three measurements are consistent with each other within the error of the measurements. We take the weighted average for these three measurements as the experimental cross section for the neutron spectrum represented in Fig. 8:

$$\sigma_{\rm exp}(^{210g}{\rm Bi}) = 1.65 \pm 0.07 \text{ mb}.$$

C. Determination of the Maxwellian averaged cross section (MACS)

The Maxwellian averaged cross section (MACS) is very useful for characterizing neutrons induced reactions. MACSs are used extensively in determining nucleosynthesis via the *s* process which occurs in stellar interiors in an environment where neutrons can be considered in thermal equilibrium at a fixed value of kT. The reaction rate for a particular process $\boldsymbol{A}$ is given by $\langle\sigma v\rangle$, the convolution of the product of the elemental cross section times the relative velocity over the distribution of neutrons at the given kT. The MACS for reaction $\boldsymbol{A}$ is defined as the reaction rate divided by the most probable velocity v_T, or

$$\sigma_{\rm MACS}(\boldsymbol{A},kT) = \frac{\langle\sigma v\rangle}{v_T} = \frac{2}{\sqrt{\pi}}\langle\sigma\rangle = \frac{2}{\sqrt{\pi}}\frac{\int_0^{\infty}\sigma(\boldsymbol{A},E_n)E_n e^{-E_n/kT}dE_n}{\int_0^{\infty}E_n e^{-E_n/kT}dE_n}, \quad (7)$$

where $\sigma(\boldsymbol{A},E_n)$ is the energy dependent cross section for reaction $\boldsymbol{A}$ initiated by neutron with energy $E_{\rm n}$. To the extent that the energy distribution of the neutrons impinging the samples resembles that of a Maxwellian-like distribution, i.e., if the actual spectrum $\frac{dn_{\rm sim}}{dE_n}$ is, to a good approximation, equal to $E_{\rm n}\times\exp(-E_{\rm n}/kT)$, then the MACS would simply be equal to $2/\sqrt{\pi}\times\sigma_{\rm exp}$ for that particular value of kT. For a more precise analysis, or if extrapolation of the MACS for a different temperature kT is desired, then the following expression for the MACS can be applied:

$$\sigma_{\rm MACS}(\boldsymbol{A},kT) = \frac{2}{\sqrt{\pi}}\sigma_{\rm exp}(\boldsymbol{A})\times C_{lib}(\boldsymbol{A},kT), \quad (8)$$

where the correction factor is given by

$$C_{lib}(\boldsymbol{A},kT) = \frac{\int_0^{\infty}\sigma_{lib}(\boldsymbol{A},E_n)E_n e^{-E_n/kT}dE_n}{\int_0^{\infty}E_n e^{-E_n/kT}dE_n} \times \frac{\int_0^{\infty}\frac{dn_{\rm sim}}{dE_n}dE_n}{\int_0^{\infty}\sigma_{lib}(\boldsymbol{A},E_n)\frac{dn_{\rm sim}}{dE_n}dE_n}. \quad (9)$$

$\sigma_{lib}(\boldsymbol{A},E_n)$ is the energy dependent cross section for reaction $\boldsymbol{A}$ initiated by neutron with energy $E_{\rm n}$, as tabulated in library *lib*, for example ENDF, JENDL, or JEFF libraries, and with the neutron flux as determined with SimLiT and GEANT4.

For activation to the ground state of ^{210g}Bi, the situation is slightly more complicated. The energy dependent cross sections $\sigma(^{210}{\rm Bi},E_n)$ listed in libraries such as ENDF, JENDL, or JEFF are for total activation to ^{210}Bi, while the measurement we performed and our experimental cross section are for activation to the ground state ^{210gs}Bi. Nonetheless, we shall assume that the scaling with neutron energy is the same for total activation of ^{210}Bi and for activation to the ^{210g}Bi ground state which corresponds to the assumption that in the energy range of interest the ratio of isomer to ground state activation cross section is constant (assumption correct for ROSFOND [41] and JEFF evaluations).

Table I lists the correction factors for the reaction ^{209}Bi$(n,\gamma)^{210}$Bi convoluted with a Maxwell-Boltzmann (MB), as compared to convolution of our simulated neutron distribution, with reaction cross sections taken from the ENDF, JENDL, and JEFF data libraries, for kT values of 35, 30, and 25 keV. The deviation of the correction factor from unity is attributed to deviation of the simulated neutron spectrum from a pure Maxwellian. As discussed above, the neutron

TABLE I. Correction factors and Maxwellian averaged cross section (MACS) for neutron activation of bismuth to ^{210g}Bi at several values of kT with extrapolations based on listed data libraries.

kT	C_{ENDF}	C_{JENDL}	C_{JEFF}	$\overline{C_{\mathrm{corr}}}$	$\sigma_{\mathrm{MACS}}(^{210g}\mathrm{Bi},kT)$ mb
35	1.010	0.871	0.865	0.915 ± 0.063	1.70 ± 0.14
30	1.022	0.978	0.960	0.987 ± 0.024	1.84 ± 0.09
25	1.080	1.134	1.110	1.11 ± 0.02	2.07 ± 0.09

spectrum is as calculated by SimLiT-GEANT4 simulation codes, where the input is the initial proton energy E_{p} and energy profile, and where the simulation includes all neutron scattering prior to incidence on the bismuth sample. While convolution of the simulated spectrum with the data libraries JEFF and JENDL result in very similar correction factors, the difference in the correction factor for the ENDF library is more prominent, especially for the higher value of kT. This difference in the correction factor is due mostly to differences of the reaction cross sections for the ENDF library, as opposed to the JEFF and JENDL libraries, in the region of the high energy tail. Differences in the correction factor between different cross section libraries have also been found in our analysis of ^{208}Pb$(n,\gamma)^{209}$Pb [30] and is attributed to the limited availability of reliable experimental data of these small cross sections which are difficult to measure not only by activation methods, but also by direct methods due to large scattering cross sections and low capture probability, especially at the higher neutron activation energies. In such a situation uncertainties in measurements and ambiguities in modeling lead to differences in evaluations. The differences between the ENDF and JENDL evaluation data libraries for the ^{209}Bi$(n,\gamma)^{210}$Bi reaction are seen in Fig. 9 which shows a plot of the evaluated cross sections in the resonance region and highlights the differences between these two evaluations at the higher neutron energies. Superimposed on Fig. 9 is the Maxwellian flux energy distribution for $kT = 35$ keV (arbitrary scale), which shows a significant overlap for regions of differences between the ENDF and JENDL cross section

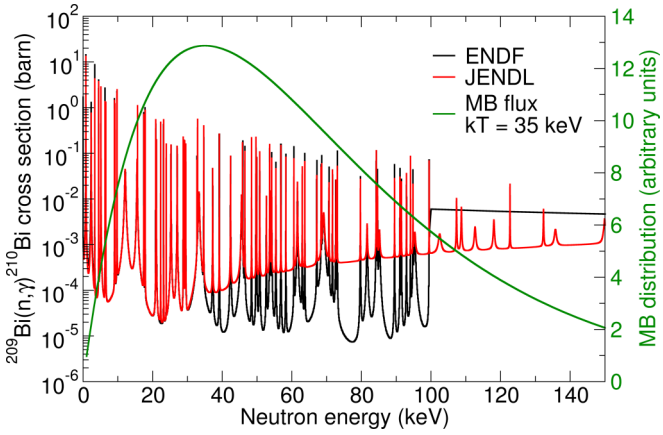

FIG. 9. ^{209}Bi$(n,\gamma)^{210}$Bi evaluated cross sections for the ENDF and JENDL data libraries (logarithmic scale) and a superimposed Maxwell-Boltzmann distribution at 35 keV (linear scale).

evaluations. The differences in the correction factors represent the error of the derived MACS due to the uncertainties in the evaluated cross sections appearing in the libraries. We therefore take as the correction factor for extracting the MACS the quantity $\overline{C_{\mathrm{corr}}}$, which is the average of the correction factors as determined with the ENDF, JEFF, and JENDL libraries, and where the error is the average of the combined differences between these libraries, as shown in Table I.

The MACS for bismuth activation inferred from our measured experimental cross section $\sigma_{\mathrm{exp}}(^{210g}\mathrm{Bi})$ are also listed in Table I for kT values of 35, 30, and 25 keV, using the correction factor average $\overline{C_{\mathrm{corr}}}$ and error as deduced from the ENDF, JEFF, and JENDL libraries. We emphasize that all previous MACS measurements extracted from activation measurements with quasi-Maxwellian neutron beams also require a correction factor to correct for the deviation of the actual neutron distribution from a pure a Maxwellian flux distribution. Inevitably, this correction can only be obtained by convolution of the obtained and desired neutron distribution with reaction cross section as obtained from reaction data libraries. The MACS result we obtain for $kT = 30$ keV is $\sigma_{\mathrm{MACS}}(^{210g}\mathrm{Bi}, kT = 30\ \mathrm{keV}) = 1.84 \pm 0.09$ mb.

V. DISCUSSION

Several measurements of neutron capture on bismuth have been reported in the past, with continuing interest given the importance for astrophysical reactions leading to the termination of the s process, and also for design criteria for GenIV reactor design, specifically radiotoxicity issues regarding Pb-Bi coolants for fast breeder reactors and targets for accelerator driven systems. Measurements of bismuth neutron capture of astrophysical significance have focused primarily on MACS at KT of 30 keV as a reference. Experiments for neutron capture to the ^{210g}Bi ground state are performed taking advantage of kinematic focusing in near-threshold Li(p,n) reactions to produce quasi-Maxweliian neutron beams, using techniques similar to those reported in this paper. Measurements using TOF techniques have been used to obtain MACSs for total neutron capture to ^{210}Bi, by measuring energy dependence reaction cross sections and subsequent convolution of these cross sections with a Maxwellian at the desired kT.

Bismuth activation with quasi-Maxwellian neutrons was reported in 2004 by Ratzel *et al.* [13], by measurement of the β decay from the ^{210g}Bi nuclei following the bismuth activation. The experiment measured neutron capture on ^{208}Pb and on ^{209}Bi, and reported on MACS measurements of 0.31 ± 0.2 mb and 2.32 ± 0.14 mb respectively, where the β's from the ^{210g}Bi decay were measured over the course of a 48-h period. Several years later, Bisterzo *et al.* [14] reported on a similar experiment involving activation of bismuth with quasi-Maxwellian neutrons, where the activation to ^{210g}Bi was determined by measuring the α activity from the ^{210}Po decay, reporting on a MACS of 2.16 ± 0.07 mb. Our measurement for bismuth activation, with a MACS of 1.84 ± 0.09 mb, is smaller than that obtained by Ratzel *et al.* and Bisterzo *et al.* Regarding the β measurement, we believe that the longer measuring time in the present work is necessary to account for β contamination from activated impurities. The α measurement should be more

TABLE II. MACS for bismuth activation at $kT = 30$ keV, our results and comparison with previous measurements.

	$\sigma_{\mathrm{MACS}}(^{210g}\mathrm{Bi})$ mb	$\sigma_{\mathrm{MACS}}(^{210\mathrm{Total}}\mathrm{Bi})$ mb
This work	1.84 ± 0.09	
Ratzel *et al.* [13]	2.32 ± 0.14	
Bisterzo *et al.* [14]	2.16 ± 0.07	
Domingo-Pardo *et al.* [10]		2.58 ± 0.50
Mutti *et al.* [11]		2.54 ± 0.48
Beer *et al.* [12]		3.12 ± 0.60

accurate, however our results are still about two standard error deviations from that measured by Bisterzo *et al.* One possible difference may be the deviation of the actual neutron energy produced in the Li(p,n) reaction, from a pure Maxwellian-like distribution, especially at higher neutron energies above 80 keV. The correction factor introduced in Eqs. (8) and (9) (see Table I) is intended to correct for this deviation of the actual neutron distribution. Furthermore, it has been shown in Ref. [37] that kinematics of the ^{7}Li(p,n) reaction with a broad energy proton beam of order $\sigma \sim 15$ keV produces neutrons with energy distribution more closely similar to that of a Maxwellian, especially in the higher energy tail region. This is the case with an RF accelerator such as SARAF, as used for our measurement, and the present spectrum may account for the lower cross section extracted.

Experiments employing TOF techniques measure capture cross sections by coincidence of detected prompt γ's with a broad energy neutron beam produced in short proton pulses of nanosecond duration provide capture cross sections for individual resonances of ^{210}Bi as a function of neutron energy. A convolution of the measured energy dependent capture cross sections with a Maxwellian distribution at the desired value of kT is employed to obtain the MACS. This latter technique provides the MACS for the total activation to ^{210}Bi, namely total capture cross section to ground state or to the metastable state ($^{210\mathrm{Total}}\mathrm{Bi} = {}^{210\mathrm{gs}}\mathrm{Bi} + {}^{210\mathrm{ms}}\mathrm{Bi}$). MACS measurements of total bismuth capture utilizing TOF techniques were first reported by Macklin and Halperin, although with insufficient resolution to separate the ^{210}Bi resonances. Beer *et al.* [12] in 1991 performed a convolution with capture cross section data, obtaining a MACS (30 keV) of 3.12 ± 0.60 mb. More recent TOF measurements include those of Mutti *et al.* [11] at the Gelina facility with a reported MACS (30 keV) = 2.54 ± 0.48 mb, and most recently of Domingo-Pardo *et al.* [10] at the nTOF facility yielding a MACS (30 keV) of 2.58 ± 0.50 mb. A comparison of the MACS measurements for bismuth neutron activation at kT of 30 keV, including our recent results, is listed in Table II. Figure 10 shows a plot of the MACS for bismuth activation to ^{210}Bi as measured by the different groups.

Of interest is the ratio $\sigma_{\mathrm{g}}/\sigma_{\mathrm{m}}$—the energy dependence of the ratio of bismuth capture cross section to the $^{210\mathrm{g}}$Bi ground-stable state as compared to capture to the $^{210\mathrm{m}}$Bi metastable state. Several experiments have reported on this ratio at various neutron energy intervals, although the errors are large and the systematics not very clear. Borella *et al.* [7] report measuring

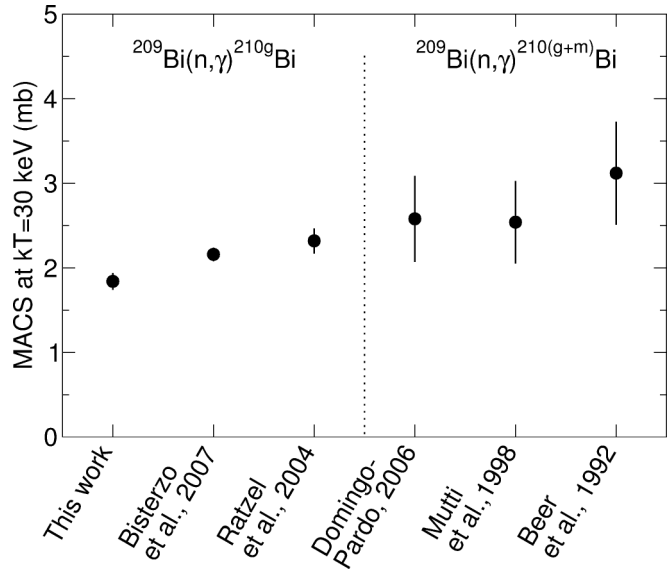

FIG. 10. Comparison of MACS at 30 keV for measurements of bismuth activation to $^{210\mathrm{g}}$Bi ground state and total activation to ^{210}Bi ($^{210}\mathrm{Bi} = {}^{210\mathrm{g}}\mathrm{Bi} + {}^{210\mathrm{m}}\mathrm{Bi}$).

a ratio of $\sigma_{\mathrm{g}}/\sigma_{\mathrm{m}} = 1.17 \pm 0.08$ with thermal neutrons. Saito *et al.* [15] report a ratio of 3 ± 2 for a broad neutron beam energy centered at 30 keV, and a ratio of 0.81 ± 0.25 for a broad neutron beam energy centered at 540 keV. Bisterzo *et al.* [14] has provided an estimate for this ratio, taking their report value for MACS at 30 keV for σ_{g}, and subtracting this from the average obtained for σ_{Total}, one obtains a ratio $\sigma_{\mathrm{g}}/\sigma_{\mathrm{m}}$ at 30 keV of 4.0 ± 2.9. The ratio for capture cross sections at various resonances from about 1 to 10 keV were measured by Borella *et al.* [39] at the Gelina facility. Evaluations of these ratios have been published by Icihara and Shibata [18], and can be derived from the ENDF or JENDL data libraries. Evaluation for the ratio $\sigma_{\mathrm{g}}/\sigma_{\mathrm{m}}$ can be found in the following libraries: Jendl/A-96 [40], Rosfond-2010 [41], Jendl-4.0 [42], Jeff-3.2 [43], and Brond-3.1 [44].

We can estimate the ratio $\sigma_{\mathrm{g}}/\sigma_{\mathrm{m}}$ at neutron energy of 30 keV by taking the average of the MACS measured for the total bismuth capture cross section (Table II), and subtracting from this average the result we have obtained for the MACS for capture to the ground state. Using the value we obtain for $\sigma_{\mathrm{MACS}}(^{210g}\mathrm{Bi})$ at kT of 30 keV and the average σ_{Total} for the values of $\sigma_{\mathrm{MACS}}(^{210\mathrm{Total}}\mathrm{Bi})$ shown in Table II, we get a ratio $\sigma_{\mathrm{g}}/\sigma_{\mathrm{m}} = \sigma_{\mathrm{g}}/(\sigma_{\mathrm{Total}} - \sigma_{\mathrm{g}}) \sim 2.14 \pm 1.07$. However, this extrapolation is very sensitive to the difference $(\sigma_{\mathrm{Total}} - \sigma_{\mathrm{g}})$, as a similar extrapolation using the MACS obtained by Bisterzo *et al.* yields a ratio of $\sigma_{\mathrm{g}}/\sigma_{\mathrm{m}} = 4.0 \pm 2.9$. Clearly, a direct measurement of σ_{m} is required.

Our original objective for this experiment was to measure γ's from the activation of the $^{210\mathrm{m}}$Bi metastable state, although this proved impractical due to high residual background of γ's produced by the ^{209}Bi$(\gamma,2n)^{207}$Bi reaction by the 14.6- and 17.6-MeV γ's produced in ^{7}Li(p,γ) reaction with thick lithium target. The bismuth samples that have been irradiated have been temporarily put aside, and we are investigating the feasibility of performing accelerator mass spectrometry

measurements with these already activated bismuth samples to detect the level of activation to ^{210m}Bi. Direct measurement of activation to the ^{210m}Bi metastable state would contribute to the certainty of the results and provide for a better understanding of the termination of the *s* process, and a better knowledge of the long lived isomer activity to address radiotoxicity issues required for more reliable planning of GenIV reactors and ADS facilities.

VI. SUMMARY

A new measurement for bismuth activation with quasi-Maxwellian neutrons is presented. The measurement was performed at the SARAF high intensity proton and deuteron RF linear accelerator and the LiLiT liquid lithium target facility, which together enable production of high flux quasi-Maxwellian neutrons. The high flux capabilities allow for sensitive measurement of small cross sections in a shorter run time, avoiding possible drifts which may occur for long run times. It has been shown in Ref. [37] that the relatively broad energy profile of the proton beam characteristic of an RF accelerator results in quasi-Maxwellian neutron distribution better fitted to a Maxwellian profile, especially in the high energy tail region. An accurate assessment of the MACS nonetheless requires detailed simulation of the reaction kinematics and the experimental environment to obtain the corrections and extrapolations needed for reliable measurements.

The experiment reported here involved measurement of activation to the bismuth ground state ^{209}Bi$(n,\gamma)^{210g}$Bi by measuring activity of β's from the ^{210g}Bi decay and α's and γ's from the subsequent ^{210}Po decay, combined with detailed Monte Carlo simulations of the ^{7}Li(p,n) reaction kinematics and the activation experimental setup. The measurements consisting of α, β, and γ detection are all consistent with each other and provide an experimental average cross section of 1.65 ± 0.07 mb. Employing SimLiT and GEANT4 simulation tools for corrections experimental kinematics and environment and ENDF, JEFF, and JENDL databases for corrections and extrapolation to the desired kT, we obtain a Maxwellian averaged cross section at $kT = 30$ keV of $\sigma_{\mathrm{MACS}}(^{210g}\mathrm{Bi}, kT = 30\ \mathrm{keV})$ of 1.84 ± 0.09 mb. This value is compared to previous measurements of activation both to the ^{210g}Bi ground state and total activation to ^{210}Bi. Our results are very similar to those previously measured Bisterzo *et al.*, and it could be that the 2σ difference reflects on the limitations of the corrections that are required to extract the MACS. An estimate for the ratio of activation to the ^{210}Bi ground state and metastable state at neutron energy of 30 keV using our results for ^{210g}B and an average of the TOF measurements for ^{210}B yields a ratio of $\sigma_g/\sigma_m = 2.14 \pm 1.07$.

ACKNOWLEDGMENTS

We would like to thank the SARAF and LiLiT operation staff for a very dedicated and helpful beam and target operation. We gratefully acknowledge the support of the the Pazi Foundation (Israel). We would like to acknowledge the help of Dr. O. Girshevitz from Bar-Ilan University in measuring the thickness of the bismuth foils using RBS techniques. We thank Prof. Peter Schillebeeckx for sharing with us the analysis of σ_g/σ_m for ^{210}Bi activation. We would also like to acknowledge the support and encouragements of the IAEC-Soreq and EC-JRC joint project initiative.

[1] D. D. Clayton and M. E. Rassbach, Astrophys. J. **148**, 69 (1967).
[2] F. Käppeler, R. Gallino, S. Bisterzo, and W. Aoki, Rev. Mod. Phys. **83**, 157 (2011).
[3] H. Schatz, R. Toenjes, B. Pfeiffer, T. C. Beers, J. J. Cowan, V. Hill, and K.-L. Kratz, Astrophys. J. **579**, 626 (2002).
[4] D. Vandeplassche and L. Medeiros Romão, *Proceedings of IPAC2012, Applications of Accelerators, Technology Transfer and Industrial Relations* (New Orleans, Louisiana, USA, IPAC12/IEEE, 2012), paper MOYAP01, p. 6.
[5] The Lund/LBNL Nuclear Data Search Version 2.0, LBNL, Berkeley, 1999, nucleardata.nuclear.lu.se/toi/.
[6] LNHB/CEA Table de Radionucleides (2014), http://www.nucleide.org/DDEP.htm, http://www.nucleide.org/Laraweb/.
[7] A. Borella, T. Belgya, S. Kopecky, F. Gunsing, M. Moxon, M. Rejmund, P. Schillebeeckx, and L. Szentmiklósi, Nucl. Phys. A **850**, 1 (2011).
[8] C. Stan-Sion, A. Letourneau, H. Reithmeier, V. Lazarev, M. Enachescu, and E. Nolte, Nucl. Instrum. Methods Phys. Res. B **259**, 739 (2007).
[9] R. Macklin and J. Halperin, Phys. Rev. C **14**, 1389 (1976).
[10] C. Domingo-Pardo *et al.* (n_TOF Collaboration), Phys. Rev. C **74**, 025807 (2006).
[11] P. Mutti, F. Corvi, K. Athanassopulos, H. Beer, and P. Krupchitsky, in *Proceedings of the International Symposium on Nuclear Astrophysics: Nuclei in the cosmos V, Volos, Greece*, edited by N. Prantzos and S. Harissopulos (Editions Frontières, Paris, 1988), p. 204.
[12] H. Beer, F. Voss, and R. R. Winters, Astrophysical J. Suppl. **80**, 403 (1992).
[13] U. Ratzel, C. Arlandini, F. Kappeler, A. Couture, M. Wiescher, R. Reifarth, R. Gallino, A. Mengoni, and C. Travaglio, Phys. Rev. C **70**, 065803 (2004).
[14] S. Bisterzo, F. Kappeler, R. Gallino, M. Heil, C. Domingo-Pardo, C. Vockenhuber, and A. Wallner, *International Conference on Nuclear Data for Science and Technology ND2007* (EDP Sciences, CEA, 2008), p. 1333.
[15] K. Saito, M. Igashira, T. Ohsaki, T. Obara, and H. Sekimoto, Proceedings of the 2002 Symposium on Nuclear Data, JAERI, Tokai, Japan, 1133 (2002) and JAERI-Conf 2003-006 JP035029.
[16] M. B. Chadwick *et al.*, Nucl. Data Sheets **112**, 2887 (2011); http://www.nndc.bnl.gov.
[17] K. Shibata, O. Iwamoto, T. Nakagawa, N. Iwamoto, A. Ichihara, S. Kunieda, S. Chiba, K. Furutaka, N. Otuka, T. Ohasawa *et al.*, J. Nucl. Sci. Technol. **48**, 1 (2011).
[18] A. Icihara and K. Shibata, J. Nucl. Sci. Technol. **40**, 980 (2003).

[19] A. Kreisel *et al.*, in *LINAC14: Proceedings of the 27th International Linear Accelerator Conference, Geneva, 2014*, edited by C. Carli, M. Draper, Y.-M. Ducimetiere, A. McCausey, R. Müller, J. Poole, and V. R. W. Schaa (CERN, Meyrin, Canton of Geneva, 2014), paper WEIOB02, p. 770.
[20] S. Halfon *et al.*, Rev. Sci. Instrum. **85**, 056105 (2015).
[21] N. Pichoff *et al.*, The SARAF-LINAC Project 2017 Status, in *Proceedings of the 8th International Particle Accelerator Conference (IPAC'17)* (Copenhagen, Denmark, 2017), pp. 2194–2196.
[22] H. Beer and F. Käppeler, Phys. Rev. C **21**, 534 (1980).
[23] L. Weissman *et al.*, JINST **10**, T10004 (2015).
[24] M. Tessler *et al.*, Phys. Lett. B **751**, 418 (2015).
[25] A. Kreisel *et al.*, Soreq Reports SNRC-4474 and SNRC-4476, available upon request.
[26] http://www.goodfellow.com/E/Bismuth-Foil.html.
[27] Bar-Ilan University RBS facility, http://nano.biu.ac.il/rbs; see for example L. Weismann *et al.*, Nucl. Instrum. Methods Phys. Res. B **342**, 7 (2015).
[28] ENDF/B-VIII.B4, U.S. Evaluated Nuclear Data Library (preliminary), 2017.
[29] C. Lederer *et al.* (n_TOF Collaboration), Phys. Rev. C **83**, 034608 (2011).
[30] L. Weissman *et al.*, Phys. Rev. C **96**, 015802 (2017).
[31] https://www.princetonscientific.com/high_purity_materials.php.
[32] http://www.canberra.com/products/radiochemistry_lab/pdf/iSolo-SS-C39505.pdf.
[33] http://www.ezag.com/home/products/isotope_products/isotrak_calibration_sources/.
[34] O. Aviv, Soreq NRC internal report (unpublished).
[35] W. Ratynski and F. Käppeler, Phys. Rev. C **37**, 595 (1988).
[36] M. Friedman *et al.*, Nucl. Instrum. Methods Phys. Res. A **698**, 117 (2013).
[37] G. Feinberg, M. Friedman, A. Krasa, A. Shor, Y. Eisen, D. Berkovits, D. Cohen, G. Giorginis, T. Hirsh, M. Paul, A. J. M. Plompen, and E. Tsuk, Phys. Rev. C **85**, 055810 (2012).
[38] http://www.geant.org/Projects/GEANT_Project_GN4.
[39] A. Borella *et al.*, International Conference on Nuclear Data for Science and Technology 2007 **ND2007**, 150 (2007).
[40] http://wwwndc.jaea.go.jp/ftpnd/jendl/jact10.html.
[41] http://www.ippe.ru/podr/abbn/english/libr/rosfond.php.
[42] http://wwwndc.jaea.go.jp/jendl/j40/j40.html.
[43] https://www.oecd-nea.org/dbdata/jeff/.
[44] https://vant.ippe.ru/en/brond-3-1.html.